A J Journal of Medical Sciences

AJ Journal of Medical Sciences

ORIGINAL ARTICLE

Folate Conjugated 5-Fluorouracil Loaded Mn_3O_4 Nanoparticles for Enhanced Efficacy of 5-Fluorouracil in Cancer Cells

Chaithra Rudrappa[1], Shaila G Sanjeevagol[2], Jayappa Manjanna[3], N Anitha[1], G T Ramya[1], M Meghana[4], E Sarathkumar[1], S J Prashanth[5], G J Sathisha[1*]

[1]*Department of Postgraduate Studies and Research in Biochemistry, Jnana Sahyadri, Kuvempu University, Shankaraghatta, Shivamogga- 577 451, Karnataka, India*

[2]*Department of Chemistry, Sangolli Rayanna First Grade Constituent College, Belagavi-590017, Karnataka, India*

[3]*Department of Chemistry, Rani Channamma University, Belagavi, 591156, Karnataka, India*

[4]*Department of Biochemistry, MMK & SDM Mahila Mahavidhyalaya, Krishanamurthypuram, Mysore- 570009, Karnataka, India*

[5]*Department of Postgraduate Studies and Research in Food Technology, Jnana Sahyadri, Kuvempu University, Shankaraghatta, Shivamogga- 577 451, Karnataka, India*

ARTICLE INFO

Article history:
Received 15-02-2026
Accepted 06-03-2026
Published 31-03-2026

** Corresponding author.*
G J Sathisha
satishlec@gmail.com

https://doi.org/10.71325/ajjms.v3i1.26.7

ABSTRACT

Background: Traditional chemotherapeutics have both beneficial and negative side effects; one effective way to mitigate the former is via targeted drug delivery systems. When it comes to malignancies that overexpress folate receptors, folic acid-mediated delivery truly emerges. A targeted anticancer nanoconjugate (Mn_3O_4-AFA-5FU NC) with enhanced cellular selectivity and therapeutic performance was developed in this study by developing and integrating an activated folic acid-5-fluorouracil conjugate with Mn_3O_4 nanoparticles (NPs). **Methodology**: Mn_3O_4 NPs were created by chemical precipitation before surface modification with the AFA-5-FU conjugate. To fully analyse the Mn_3O_4-AFA-5FU nanoconjugates (NCs), we used Fourier-transform infrared spectroscopy, ultraviolet-visible spectroscopy, and scanning electron microscopy. This enabled us to verify that the NCs preserved their morphological integrity, the NPs were properly synthesized, and the surface functionalization was successful. We then examined their ability to inhibit the growth of HeLa human cervical cancer cells. In a controlled laboratory setting, the MTT assay was used to assess the cytotoxic effects of Mn_3O_4-AFA-5FU (3.1-100 µg/mL) with serial tenfold dilutions on HeLa cells. Cell migration, DNA damage, Caspases-3, 8 and 9 activities, alkaline Comet test, and scratch assay tests were utilized to evaluate the treated cells' effects on cell cycle arrest, DNA damage, and fragmentation, respectively. **Result**: The findings indicated that Mn_3O_4-AFA-5FU NCs were much more cytotoxic than Mn_3O_4 NPs and 5-FU, exhibiting an IC_{50} of 1.681 µg/mL. Flow cytometry indicates that the cells persist in the G2/M and S phases of the cell cycle, but the quantity of sub-G0/G1 cells is increasing. DNA fragmentation and caspase analysis demonstrated substantial apoptosis, signifying the activation of the extrinsic apoptotic pathway. The scratch assay exhibited a significant reduction in cancer cell migration. **Conclusion**: In conclusion, folate-mediated targeting and nanoparticle-based drug delivery significantly enhance medication availability within cells and their therapeutic efficacy. Mn_3O_4-AFA-5FU NCs may serve as a viable platform for targeted cancer therapy.

Keywords: Mn_3O_4 nanoparticles; Folic acid targeting; 5-Fluorouracil; Apoptosis; Caspase activation; Targeted drug delivery

INTRODUCTION

Women living in underdeveloped nations are at a disproportionately higher risk of acquiring cervical cancer due to restricted access to early preventative measures. Cervical cancer continues to be a significant health challenge for women all over the world. The anti-tumour medications that are now available have a number of negative characteristics, including the fact that they are frequently toxic, have little efficacy, and lead to the development of drug resistances[1-2]. The existence of these restrictions highlights how essential it is to investigate alternative therapeutic techniques that have the potential to enhance treatment outcomes while simultaneously lowering systemic toxicity. One of the most well-known chemotherapeutic agents, 5-fluorouracil, is employed in the treatment of a variety of carcinomas, including breast, lung, cervical, and colorectal carcinomas[3]. The inhibition of thymidylate synthase by 5-FU has been demonstrated to be responsible for its antiproliferative effect. This inhibition results in disruptions in DNA synthesis, which in turn leads to cell-cycle arrest and apoptosis[4]. Unfortunately, it is known to have a rapid metabolism, low specificity to target cancer cells, low bioavailability, and systemic toxicity in a dose-dependent manner[5-6]. As a result, researchers have been exploring various carrier-mediated drug delivery systems in an effort to improve the stability of 5-fluorouracil, as well as its bioavailability and specificity to target cancer cells. Drug delivery systems that are based on nanotechnology provide viable answers to the limits of conventional chemotherapy. These technologies improve pharmacokinetics, enable controlled drug release, and enhance tumour targeting[7-8], which are all important aspects of chemotherapy. Metal oxide NPs, in particular Mn_3O_4 NPs, have attracted interest because of their redox activity, biocompatibility, and physicochemical stability; these properties enable them to modulate intracellular oxidative stress and boost anticancer responses[9-10]. A further improvement in the selectivity and therapeutic efficacy of nanoparticle-mediated drug delivery can be achieved through the utilization of active targeting techniques. Folic acid (FA) is frequently used because folate receptors are overexpressed in many malignancies, including cervical carcinoma, while they are poorly expressed in normal tissues[11-12]. This allows therapeutic selectivity to be further improved through active targeting, which is a method that can be used to improve therapeutic selectivity. Nanocarriers that are functionalized with FA take advantage of receptor-mediated endocytosis, which leads to greater cellular uptake and cytotoxicity as compared to systems that are not targeted[13-14]. It is abundantly clear that the purpose of the current research is to design and synthesize the activated form of folic acid that has been conjugated to 5-FU and then further conjugated to the Mn_2O_3 nanoparticles in the form of nanoconjugates. These nanoconjugates have the potential to be beneficial as a nanoscale anticancer drug delivery system. For the purpose of characterizing the nanoconjugates that were produced, techniques such as FT-IR, SEM, and UV-visible spectroscopy were utilized. Using human cervical carcinoma cells, the in vitro anticancer activity of the synthesized NC was evaluated using a number of different biological assays. These assays included an MTT-based cytotoxicity assessment, an analysis of cell-cycle distribution, an evaluation of caspase-mediated apoptosis, a comet assay for DNA damage analysis, and a scratch assay for cell migration. Since this is the case, the purpose of the current research is to determine whether or not Mn_2O_3-AFA-5FU-NCs have the ability to serve as a targeted drug delivery system in the context of anticancer treatment.

MATERIALS AND METHODS

Materials

All of the chemicals that were used were obtained from Sigma-Aldrich in Bangalore, India. These chemicals included sodium hydroxide (NaOH), Manganese chloride tetrahydrate ($MnCl_2{\cdot}4H_2O$), and 5-fluorouracil (5-FU). There was no extra purification processes performed on these compounds. Folic acid, N-Hydroxysuccinimide (NHS), dicyclohexylcarbodiimide (DCC), methanol, diethyl ether, and dimethyl sulfoxide (DMSO) were among the analytical-grade chemicals that we went out and purchased from HiMedia Laboratories in Bangalore, India.

Synthesis and Conjugation

Synthesis of Mn_3O_4 Nanoparticles

A 0.5 M manganese (II) precursor solution was made by dissolving $MnCl_2{\cdot}4H_2O$ in Milli-Q water. A 10% (w/v) NaOH solution was added drop wise with continuous magnetic stirring for roughly 4 hours until the pH approached 10, causing precipitate formation. The reaction mixture had been stirred for an additional 12 hours at room temperature to allow for growth in the mother liquor. The precipitate was collected by filtering, washed several times with Milli-Q water, and dried at 90°C for 24 hours. The final product is known as as-prepared Mn_3O_4 NPs.

Activation of Folic Acid

Folic acid was activated using carbodiimide chemistry, as previously described[15-16]. Folic acid (0.884 g) was dissolved in 20 mL DMSO using sonication for 30 minutes. DCC (0.784 g) and NHS (0.256 g) were added sequentially, followed by triethylamine (1 mL), and the reaction mixture was agitated for 24 hours at room temperature in the dark. The dicyclohexylurea by-product

was filtered away, and the residual material was treated with 30% acetone in diethyl ether to separate the AFA. The result was properly rinsed with diethyl ether, dried, and kept for future use.

Preparation of AFA-5FU conjugates

Activated folic acid and 5-FU, each weighing 0.1 g, were dissolved in 20 mL of milli-Q water and left to react for 24 hours at room temperature while constantly stirring. Afterward, the reaction mixture was centrifuged at 5000 rpm for 30 minutes. The conjugate-containing pellet was then purified employing dialysis with a 3.5 kDa molecular weight cut-off membrane. This operation took 6 hours, with the milli-Q water being replenished every hour. Finally, the leftover conjugate was washed, centrifuged, and vacuum-dried at 40°C for 24 hours to provide the AFA-5FU conjugate.

Conjugation of AFA-5FU with Mn_3O_4 Nanoparticles

Mn_3O_4 NPs (25 mg) and AFA-5FU conjugate (25 mg) were dispersed in 10 mL of Milli-Q water and magnetically swirled for 2 hours to ensure uniform mixing. The suspension was to be incubated on a rotary shaker at 200 rpm for 24 hours to enhance surface conjugation. After incubation, the mixture was centrifuged at 8000 rpm for 20 minutes to collect Mn_3O_4-AFA-5FU NCs. The pellet was washed with Milli-Q water to remove unbound conjugate, and then lyophilized for 48 hours to get the final Mn_3O_4-AFA-5FU NCs.

Evaluation of Nanoparticle Attributes

The UV-visible spectra of 5-FU, folic acid, bare Mn_3O_4 NPs, AFA, AFA-5FU conjugate, and Mn_3O_4-AFA-5FU NCs were recorded using a UV-visible spectrophotometer between 200 and 800 nm. Milli-Q water was employed as the baseline reference, and the samples were dispersed in it and analysed using a quartz cuvette with a path length of 1 cm.

Functional groups were identified and conjugation was verified using Fourier Transform Infrared spectroscopy (FTIR). The desiccated samples were combined with KBr powder and pressed into pellets. The background was corrected using purified KBr, and the spectra were measured within the 4000-400 cm^{-1} range.

Scanning electron microscopy (SEM) was employed to evaluate particle size and surface morphology. The samples were imaged under high-vacuum conditions after being affixed on carbon tape and sputter-coated with a conductive layer. Based on Feret diameter measurements, ImageJ software was employed to conduct particle size analysis.

Cell Culture

The cell lines, including HeLa (human cervical cancer cells), were obtained from the National Centre for Cell Science (NCCS) in Pune, India. Cells were routinely maintained in DMEM/F12 media (Gibco, USA) supplemented with 10% heat-inactivated fetal bovine serum (FBS), 1% penicillin-streptomycin (100 U/mL penicillin and 100 µg/mL streptomycin), and 1% L-glutamine at 37°C in a humidified environment containing 5% CO. The culture media was replenished every 2-3 days, and the cells were sub cultured at 80% confluence with 0.25% trypsin-EDTA. They were periodically tested for microbiological contamination and cell morphology.

MTT-based Cytotoxicity Assessment

The cytotoxicity of produced NPs and NCs was determined in HeLa cells using the MTT assay[17]. HeLa cells were seeded in 96-well plates (1×10^4 cells/well) and exposed to Mn_3O_4 NPs, 5-FU, and Mn_3O_4-AFA-5FU NCs via serial dilution from 0 to 100 µg/1 mL (one-fold dilution) for 48 hours. MTT reagent (5 mg/mL in PBS, 10 µL/well) was used and incubated for 4 hours. The formazan crystals were solubilized using DMSO. The absorbance of the produced colour was measured at 570 nm. Data are presented as mean ± SD from triplicate experiments. The % viability was estimated relative to the control using **Eq. (1)**, and IC_{50} values were established by nonlinear regression using GraphPad Prism (v10.10). Statistical analysis was performed using one-way ANOVA and Dunnett's test, with a significance threshold of $p < 0.05$.

$$\% \text{ Cell viabilty} = \frac{\text{Absorbance of treated cells}}{\text{Absorbance of control cells}} \times 100 \qquad (1)$$

Analysis of Cell-Cycle Distribution Using Flow Cytometry

Using vehicle-treated cells as a control, HeLa cells were seeded under usual culture conditions and treated with MnO_4-AFA-5FU NCs at the IC_{50} concentration. To remove RNA interference, cells were taken after exposure, fixed with ethanol, and stained with propidium iodide. The distribution of cells across the cell cycle stages was evaluated using the BD FACS Calibur flow cytometer based on fluorescence intensity, and data was gathered using the BD Cell Quest Pro software (v6.0). Two-way ANOVA and Tukey's multiple comparisons test were used for statistical analysis in order to evaluate the differences between the control and treatment groups in each cell-cycle phase. At $p < 0.05$, differences were deemed statistically significant.

Quantifying Caspase-3, -8, and -9 Activities

Caspase-3, 8, and 9 activities were assessed using the Caspase colorimetric assay kit (Elabscience) according to

the manufacturer's instructions. Cells were cultivated on multi-well plates and subjected to Mn_3O_4-AFA-5FU NCs at IC_{25}, IC_{50}, and IC_{100} concentrations for 24 hours. Untreated cells were used as controls. After treatment, cells were washed, collected, lysed, and centrifuged to extract protein. An equivalent amount of protein was combined with reaction buffer and caspase-3, caspase-8, and caspase-9 chromogenic substrates (Ac-DEVD-pNA, Ac-IETD-pNA, and Ac-LEHD-pNA, respectively). Substrate hydrolysis was measured at 405 nm using a microplate reader, and caspase activity was assessed in comparison to control cells. Statistical analysis was performed using one-way ANOVA and Dunnett's post-test, with p-values < 0.05 considered significant.

Alkaline Comet Assay for DNA Damage Assessment

DNA damage in HeLa cells treated with 5-FU and MnO_4-AFA-5FU NCs at their IC_{50} concentrations was assessed using the alkaline comet assay[18], while untreated cells were used as controls. Following treatment, cells were lysed, embedded in agarose, and electrophoresed in an alkaline environment. After neutralizing and staining the slides with a fluorochrome specific to nucleic acids, comet images were taken with an epifluorescence microscope. Using Open Comet (ImageJ) software, DNA damage was measured and recorded as a percentage of DNA in the tail and Olive tail moment[19]. Each slide had at least 50 cells. One-way ANOVA and Dunnett's test were employed for statistical analysis, and a p-value of less than 0.05 was deemed significant.

Cell Migration Evaluation Using the Scratch Assay

The scratch-assay was used to evaluate MnO_4-AFA-5FU's inhibitory effect and cell migratory behaviour. After seeding and growing the cells to confluence in six-well plates, a sterile 50 µL pipette tip was used to make a linear scratch. After gently washing the detached cells with PBS, the cultures were incubated under usual conditions with control, 5-FU, or MnO_4-AFA-5FU. Using an inverted microscope, phase-contrast pictures were taken at 0, 6, 12, 18, 24, and 30 hours. ImageJ (v1.54p) was used to quantify scratch closure, and **Eq. (2)** was used to express migration as a percentage of scratch closure. Dunnett's test and one-way ANOVA were used for statistical analysis, and $p < 0.05$ was deemed significant[20].

$$\textbf{Cell migration}\ (\%) = \frac{(A_0 - A_t)}{A_0} \times 100 \qquad (2)$$

Where A_t stands for the scratch area at the relevant time point and A_0 for the scratch area measured at 0 hours.

Statistical Analysis

All experiments were conducted in triplicate. The data is presented as the mean ± standard deviation. GraphPad Prism version 10.1.0 (GraphPad Software, San Diego, CA, USA) was employed to conduct statistical analyses. Statistical significance was determined at $p < 0.05$, and differences between groups were analysed using one-way or two-way ANOVA, followed by Tukey's post hoc test, Dunnett's test, and nonlinear regression.

RESULTS

Confirmation of the Formation and Conjugation of Mn_3O_4 Nanoparticles

Mn_3O_4 NPs were synthesized through an initial hydroxide precipitation, which was subsequently followed by an oxidative transformation. The chemical reactions involved in the formation of Mn_3O_4 are summarized in **Eq. (1-2)**. During this process, Mn^{2+} ions reacted with hydroxide to generate $Mn(OH)_2$, which subsequently went through oxidation and dehydration to yield mixed-valence Mn_3O_4 containing Mn^{2+} and Mn^{3+} species. Effective surface modification was demonstrated by the emergence of functional group bands associated with folic acid activation and 5-FU conjugation, as well as the confirmation of successful synthesis and surface functionalization through UV-Vis and FTIR analyses. These analyses revealed characteristic manganese oxide features. The SEM imaging revealed uniformly distributed nanoscale particles with minimal agglomeration, and the preserved morphology after conjugation confirmed that surface functionalization did not compromise the structural integrity of the nanoparticles.

$$Mn^{2+} + 2OH^- \rightarrow Mn(OH)_2 \qquad (1)$$

$$6Mn(OH)_2 + 2O_2 \rightarrow 2Mn_3O_4 + 6H_2O \qquad (2)$$

Characterization

The UV–visible spectra of 5-FU, AFA, AFA–5FU, Mn_3O_4 NPs, and Mn_3O_4-AFA-5FU NCs are presented in Fig. 1(A). The free 5-FU exhibited a UV absorption band at 265 nm, characteristic of π–π* transitions within the pyrimidine ring. AFA exhibited a wide absorption band about 280 nm and 350 nm, attributable to its aromatic chromophores. The AFA–5FU combination exhibited combined characteristics of both components with increased intensity, validating successful molecular linking. Bare Mn_3O_4 nanoparticles exhibited extensive absorption in the ultraviolet spectrum, characteristic of metal oxide nanoparticles. Following surface functionalization and drug loading, the Mn_3O_4-AFA-5FU nanoconjugates exhibited enhanced absorbance, spectrum broadening, and overlapping bands indicative of both AFA

and 5-FU, thereby confirming effective conjugation and the establishment of a stable targeted nanoconjugate system.

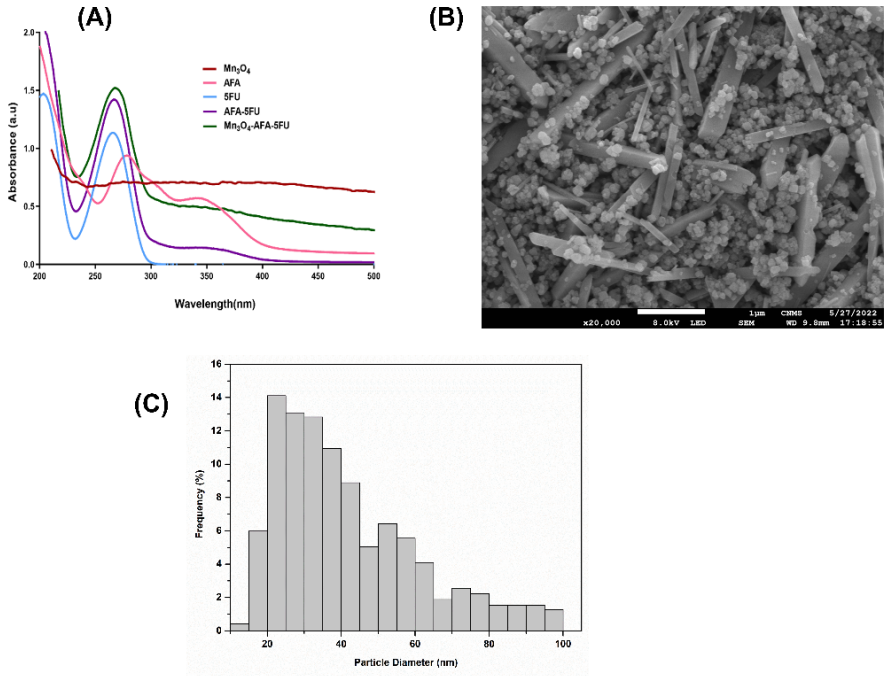

Fig. 1: (A) UV-visible absorption spectra of 5-FU, AFA, bare Mn_3O_4 nanoparticles, AFA-5FU, and Mn_3O_4-AFA-5FU nanocomposites. (B) SEM micrograph illustrating nanoscale morphology. Histogram of particle size distribution derived from Feret diameter measurements of 1169 individual nanoparticles utilizing ImageJ software

The SEM images (Fig. 1(B)) indicate that Mn_3O_4 NPs are predominantly spherical with smooth surfaces and moderate agglomeration, a characteristic that is frequently observed in wet-chemically synthesized oxide nanomaterials. The well-resolved individual particles corroborate growth and successful nanoscale nucleation, resulting in discrete Mn_3O_4 nanospheres rather than irregular aggregates. To analyse the particle size and distribution, ImageJ software was employed, with a primary focus on the 20–45 nm range, as illustrated in Fig. 1(C). A minor tail toward larger sizes suggests mild polydispersity. The average particle diameter was 41.55 ± 19.35 nm (n = 1169). The suitability of Mn_3O_4 NPs for subsequent surface functionalization and conjugation is demonstrated by the minimal aggregation and limited nanoscale distribution.

The FTIR spectrum of Mn_3O_4 NPs, as illustrated in Fig. 2, exhibits the typical Mn-O stretching vibrations within the 400–650 cm^{-1} range, thereby verifying the formation of the oxide lattice. The successful NHS activation of folic acid is indicated by the presence of characteristic bands in AFA that correspond to –OH/–NH stretching, carbonyl groups, and amide vibrations. The drug's structural integrity is confirmed by the spectrum of 5-FU, which exhibits its typical N-H and C=O stretching and ring vibration bands.

The AFA-5FU spectrum maintains the primary characteristics of both components after conjugation, with significant modifications in the carbonyl and amide regions, indicating the establishment of an amide linkage between AFA and 5-FU. The organic functional group vibrations of AFA-5FU are also evident in the Mn_3O_4-AFA-5FU NCs, with minor shifts and attenuation, while the characteristic Mn-O bands are retained. The interfacial interactions between the conjugate and the nanoparticle surface are reflected in these spectral changes. The successful anchoring of AFA-5FU onto Mn_3O_4 NPs is confirmed by the simultaneous presence of Mn-O vibrations and distinct carbonyl/amide features, which validates the formation of the targeted nanotherapeutic system.

MTT-Based Cytotoxicity Analysis

The MTT assay was used to determine the cytotoxic effect of Mn_3O_4 NPs, 5-FU, and Mn_3O_4-AFA-5FU NC. Mn_3O_4-AFA-5FU NCs dramatically reduced cell viability compared to Mn_3O_4 NPs and 5-FU alone (Fig. 3). The IC_{50} values (Table. 1) support the improved cytotoxicity of NC compared to 5-FU. At a lower concentration (3.1 µg/mL), Mn_3O_4-AFA-5FU NCs significantly reduced cell

viability by 35% compared to Mn_3O_4 NPs (roughly 70%) and free 5-FU (nearly 85%) ($p < 0.001$). The Mn_3O_4-AFA-5FU NC dramatically increased cytotoxicity at all doses tested. Mn_3O_4 NPs exhibited mild cytotoxicity, while 5-FU demonstrated better cell survival at greater doses. Statistically significant effects were observed across all treatment groups (*$p < 0.05$ to ***$p < 0.001$).

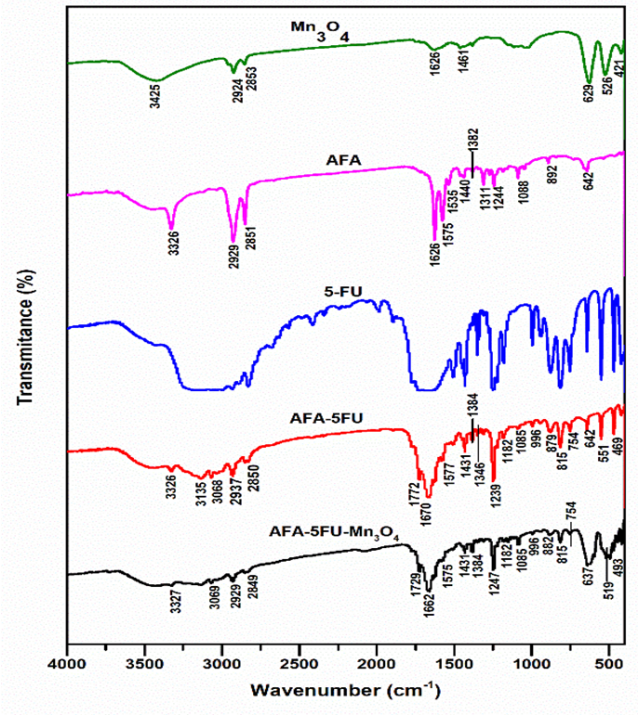

Fig. 2. FTIR spectra of Mn_3O_4 NPs, AFA, 5-FU, AFA-5FU complex, and Mn_3O_4-AFA-5FU NC, which corroborate successful surface functionalization and illustrate functional group interactions

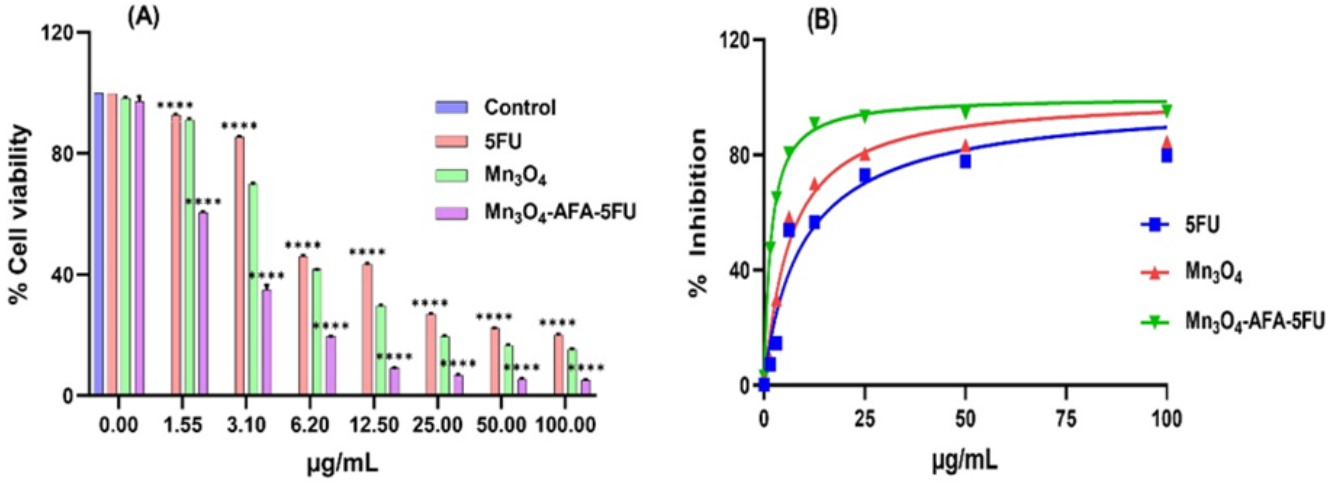

Fig. 3: Effect of 5-FU, Mn_3O_4 NPs, and Mn_3O_4-AFA-5FU NCs on cell survival. (A) MTT assay assessed the percentage of cell viability after 48 hours of treatment at the respective concentrations. (B) Corresponding dose-response curves with % inhibition for IC_{50} determination

Table 1: IC_{50} values determined by MTT assay

Treatment	IC_{50} (µg/mL)
5-FU	9.98 ± 0.05
Mn_3O_4 NPs	6.380 ± 0.03
Mn_3O_4-AFA-5FU NCs	1.681 ± 0.01

Table 2: Cell-cycle phase distribution of HeLa cells following treatment with Mn_3O_4-AFA-5FU NCs

Phase	Control (%)	Mn_3O_4-AFA-5FU (%)	p-value
Sub-G_0/G_1	2.78 ± 0.19	5.66 ± 0.05	$p < 0.0001$
G_0/G_1	69.63 ± 0.34	53.27 ± 0.11	$p < 0.0001$
S	5.80 ± 0.09	6.21 ± 0.04	$p < 0.01$
G_2/M	22.05 ± 0.10	34.86 ± 0.16	$p < 0.0001$

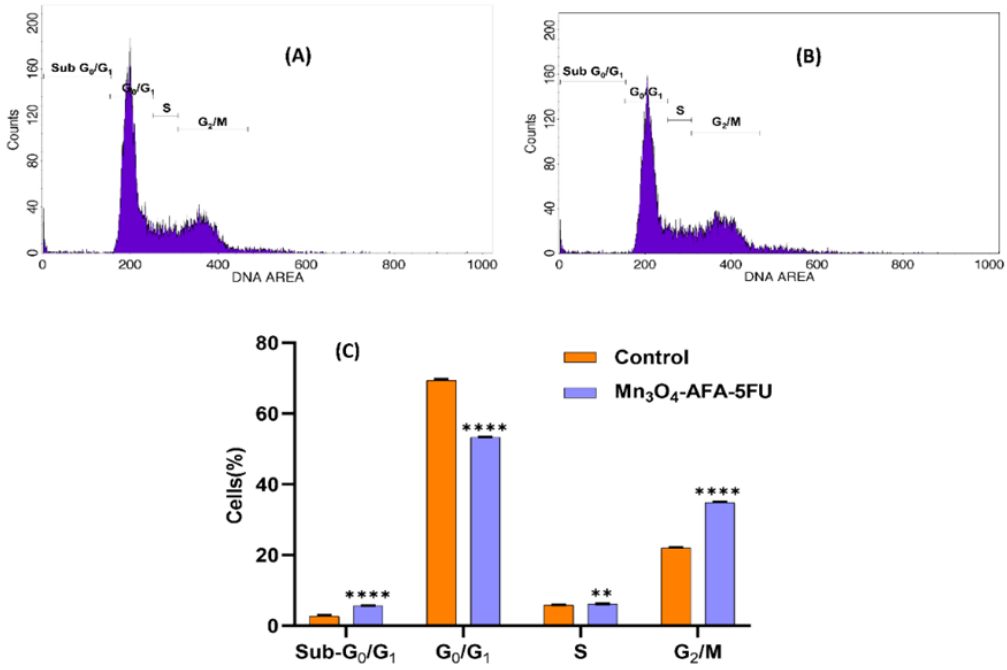

Fig. 4: Cell cycle examination of HeLa cells. (A) A representative propidium iodide (PI) fluorescence histogram of untreated HeLa cells. (B) A PI histogram of HeLa cells treated with Mn_3O_4-AFA-5FU NCs for 24 hours. (C) The quantitative distribution of cells in sub-G_0/G_1, G_0/G_1, S, and G_2/M stages after treatment

Distribution of Cell Cycles Phases after Treatment

When compared to the control group, the cell cycle profile following treatment with Mn_3O_4-AFA-5FU revealed a notable phase distribution shift (Fig. 4). The Sub-G_0/G_1 phase significantly increased in treated cells, suggesting significant DNA breakage and death. Along with a significant accumulation of treated cells in the G_2/M phase and a slight increase in the S phase, the observed results also show a significant reduction in the G_0/G_1 phase, which suggests the inhibition of normal cell cycle progression. These findings suggest that Mn_3O_4-AFA-5FU causes replication stress and cell cycle arrest primarily at the G_2/M phase. When combined, these results suggest that Mn_3O_4-AFA-5FU dramatically inhibits the progression of the cell cycle and triggers apoptosis, offering a molecular explanation for its enhanced anticancer effect.

Caspase-Induced Apoptotic Activity

Caspase-3 activity increased gradually from baseline to 74.94 ± 0.79, 90.22 ± 0.59, and 96.97 ± 0.63 nM at IC_{25}, IC_{50}, and IC_{100} dosages, respectively ($p < 0.0001$), indicating efficient apoptosis execution. Caspase-8 activity increased considerably at the same doses, reaching 69.08 ± 2.76, 118.16 ± 2.08, and 168 ± 2.38 nM ($p < 0.0001$), indicating activation of the extrinsic apoptotic pathway. Caspase-9, on the other hand, showed a less dramatic increase than the other two, indicating a less contribution from the intrinsic pathway. The results in Fig. 5 demonstrate that Mn_3O_4-AFA-5FU NCs cause cell death through the extrinsic pathway.

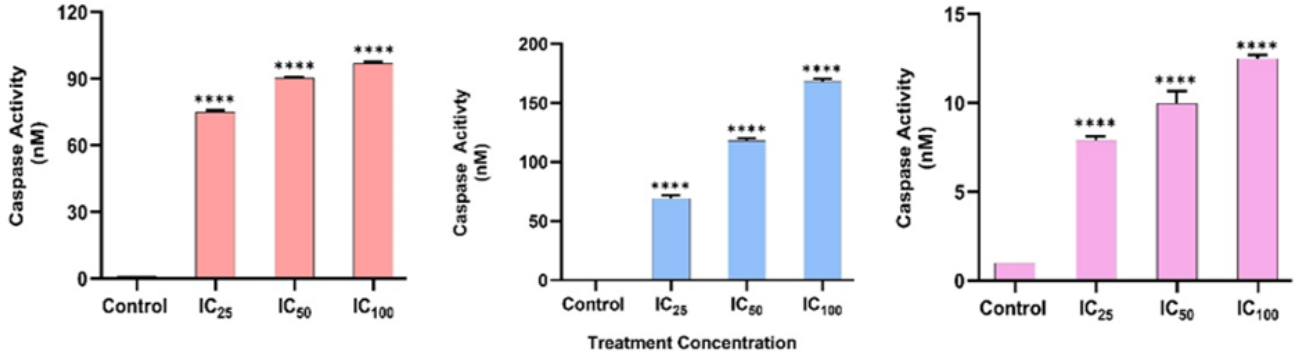

Fig. 5: Caspase activation in HeLa cells subsequent to treatment with Mn_3O_4-AFA-5FU NCs. Caspase-3, caspase-8, and caspase-9 activities were assessed following exposure to IC_{25}, IC_{50}, and IC_{100} concentrations

Assessment of DNA Damage Using Comet Assay

DNA damage was assessed using an alkaline comet assay with exposure to 5-FU and Mn_3O_4-AFA-5FU NC at respective IC_{50} values. Control cells have intact nucleus morphology and almost minimal DNA migration, indicating normal genomic integrity. Cells treated with 5-FU showed considerable DNA fragmentation, as shown by a percentage of DNA in the tail (39.66 ± 4.93) and an Olive tail moment (8.41 ± 0.98). Similarly, cells treated with Mn_3O_4-AFA-5FU NC revealed a degree of damage, with a percentage DNA in the tail (38.61 ± 8.50) and an Olive tail moment (8.50 ± 1.17). Both treatments caused significant DNA damage; relatively minor variations in the Olive tail moment may be related to differences in DNA migration behaviour, which could represent intracellular drug action or chromatin interactions, as seen in Fig. 6. DNA Damage Evaluation by Comet Assay.

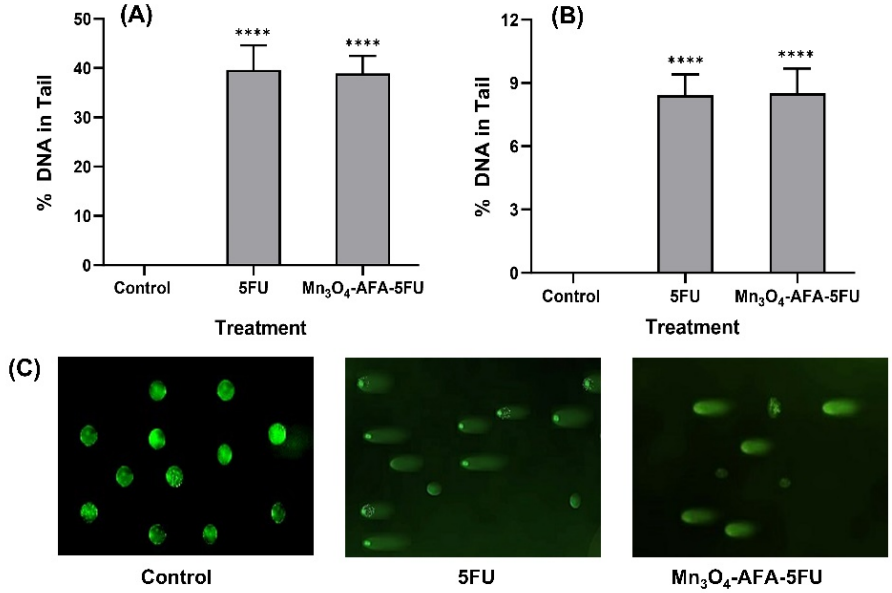

Fig. 6: Alkaline comet test for assessing DNA damage in HeLa cells. (A) Tail DNA percentage and (B) Olive tail moment in cells treated with control, 5-FU, and MnO_4-AFA-5FU at IC_{50} doses. 50 µm is the scale bar

Impact on the Migration of Cells

Following treatment with 5-FU and Mn_3O_4-AFA-5FU NC, the migratory effect of HeLa cells was assessed using the scratch assay, as illustrated in Fig. 7. In untreated cells, the analysis showed increasing scratch closure, suggesting active migration. Beginning at 12 hours, both 5-FU and Mn_3O_4-AFA-5FU NC markedly impeded scratch closure when compared to control, with the NC exhibiting a stronger inhibitory impact, as shown by quantitative evaluation. After 48 hours, cells treated with 5-FU only

partially healed (62.92 ± 0.47, $p < 0.0001$), while cells treated with NC showed the least amount of closure (70.68 ± 0.56, $p < 0.0001$). In contrast, control scratch had almost full closure (98%) after 48 hours. These findings demonstrate that Mn_3O_4-AFA-5FU NCs may interfere with tumour invasion and metastasis processes by efficiently inhibiting cancer cell migration.

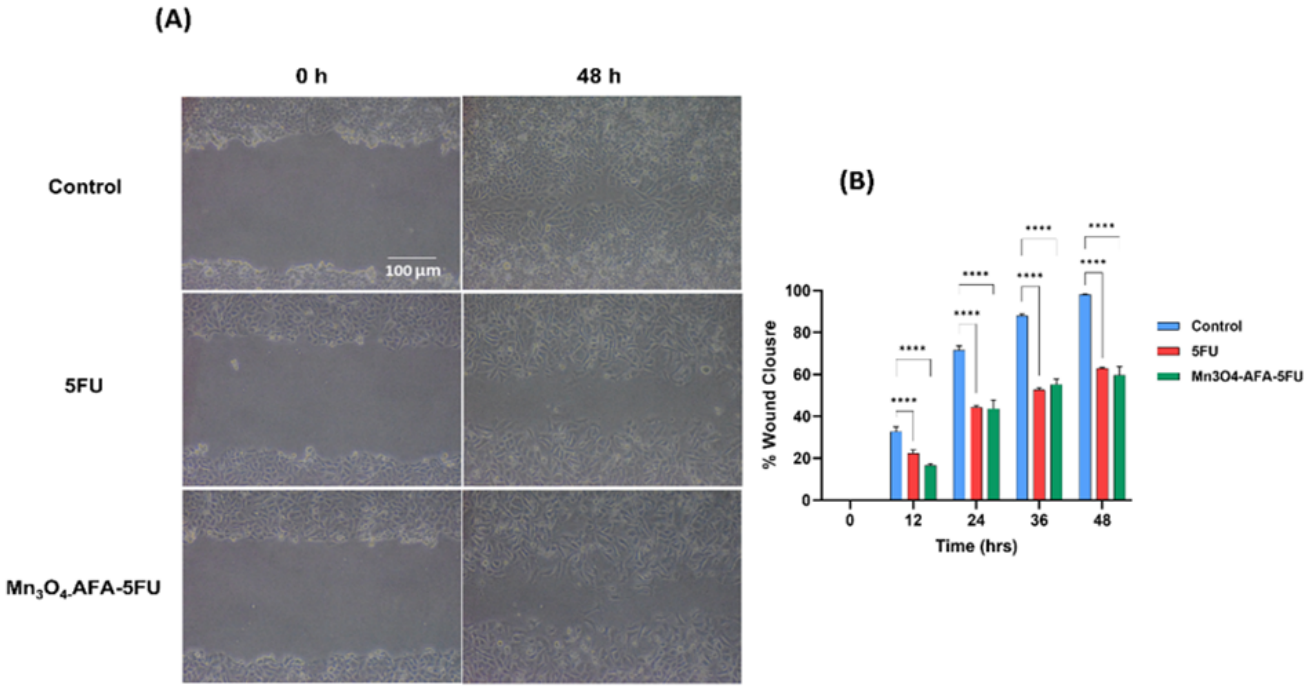

Fig. 7: (A) The scratch assay's representative phase-contrast images at 0 and 48 hours demonstrate cell movement in control, 5-FU, and Mn_3O_4-AFA-5FU NC treated cells. (B) Quantitative evaluation of scratch closure over time, shown as a percentage. 100 µm is the scale bar

DISCUSSION

The objective of this study was to evaluate the anticancer potential of a Mn_3O_4 nanocarrier system by conducting detailed physicochemical and biological investigations and to construct a targeted drug delivery system using an AFA-5-FU conjugate. The FA was initially chemically activated and subsequently conjugated with 5-FU. Subsequently, the AFA-5FU conjugate was finalized by association with Mn_3O_4 NPs to produce the Mn_3O_4-AFA-5FU NCs, as demonstrated by spectroscopic and morphological analysis. The FA's incorporation provides a targeting moiety for folate receptor–overexpressing cancer cells, while Mn_3O_4 NPs offer a robust nanoscale substrate for drug loading and delivery. Collectively, the findings indicate that the engineered NC exhibits substantially enhanced biological activity, effective surface functionalization, and strong, robust structural integrity when contrasted with the 5FU and bare Mn_3O_4 NPs.

The UV–visible absorption spectrum of Mn_3O_4 NPs demonstrated a profile that was consistent with previous research on Mn_3O_4 nanostructures, thereby validating the effective synthesis of the NPs using the employed precipitation method. The key form for efficient functionalization and cellular interaction was disclosed by SEM images, which demonstrated that NPs were evenly distributed without aggregation or morphological irregularities. The retention of Mn–O vibrational modes confirmed the preservation of the oxide core, while FTIR spectral shifts and attenuation of carbonyl- and amine-associated bands following conjugation indicated chemical bonding rather than mere physical adsorption.

The Mn_3O_4-AFA-5FU- NC confirmed the increased cytotoxicity, as evidenced by lower IC_{50} values compared to 5-FU, thereby suggesting the enhanced therapeutic efficiency. This improved activity is likely the result of protracted intracellular drug retention and improved cellular uptake, which is facilitated by folate receptor targeting. Mechanistically, the Mn_3O_4-AFA-5FU NC effectively disrupts cell cycle progression and induces apoptotic cell death, as evidenced by a significant increase in the Sub-G_0/G_1 population and G_2/M phase arrest, as revealed by cell cycle analysis. These findings were further corroborated by caspase assays, which demonstrated the activation of caspase-3, -8, and -9 in a dose-dependent manner. The nanoconjugate's coordinated and efficient cell death response is underscored by the significant increase in caspase-8 in comparison to caspase-9, which indicates a predominantly engaged extrinsic

apoptotic pathway. Additionally, the activation of caspase-3 confirms the execution of apoptosis.

Genotoxicity, as assessed by the alkaline comet assay, demonstrated that Mn_3O_4-AFA-5FU NC induces DNA damage comparable to 5-FU at IC_{50} concentrations, as indicated by comparable % DNA in tail and Olive tail moment values. The observed variation in DNA migration behaviour may be indicative of differences in intracellular drug release dynamics or chromatin interactions, indicating that nanoformulation affects the spatial presentation of DNA damage while maintaining cytotoxic efficacy. Additionally, the Mn_3O_4-AFA-5FU NC demonstrated a substantial inhibition of HeLa cell migration in the scratch assay, surpassing the effect of 5-FU. The capability of Mn_3O_4-AFA-5FU NC to disrupt cellular motility, a critical factor in tumour invasion and metastasis, is underscored by the substantial inhibition of scratch closure.

These results suggest that Mn_3O_4-AFA-5FU NC is a single nanosystem that integrates the targeted delivery, improved cytotoxicity, effective apoptosis induction, genotoxic stress, and anti-migratory effect. This convergence effect emphasizes the therapeutic benefits of the NC in comparison to the drug alone and substantiates its potential as a multifunctional platform for targeted cancer therapy.

CONCLUSIONS

The findings of this investigation demonstrate the effective synthesis of MnO_4-AFA-5FU NC and support its multipurpose anticancer potential. The successful production of MnO_4 NPs and the efficient surface functionalization of AFA and 5FU to the MnO_4 NP were verified by physico-chemical characterization. According to in-vitro research, the Mn_3O_4-AFA-5FU NC exhibited more cytotoxicity than 5-FU because of enhanced cellular uptake and prolonged intracellular drug availability. According to the results of the comet assay, the NC effectively suppressed the advancement of the cell cycle, caused a considerable amount of caspase-mediated apoptosis, and preserved the genotoxic efficiency of 5-FU. Additionally, it significantly inhibited the migration of cancer cells, emphasizing the disruptive mechanism behind tumour invasion and metastasis. Together, these findings demonstrate the therapeutic benefit of the customized nanosystem and support its promise as a potent and adaptable platform for state-of-the-art cancer treatment.

DISCLOSURE

Conflict of Interest: None.

Acknowledgement: The authors sincerely acknowledge the Department of Science and Technology (DST), Government of India, for supporting the establishment of instrumentation facilities at the Department of Biochemistry, Kuvempu University, Shankaraghatta, Karnataka, under the 'Fund for Improvement of Science and Technology' (FIST) program (Grant No. SR/FST/LS-1/2018/175(C)), which greatly facilitated the successful completion of this study.

References

1. Bray F, Ferlay J, Soerjomataram I, Siegel RL, Torre LA, Jemal A. Global cancer statistics 2018: GLOBOCAN estimates of incidence and mortality worldwide for 36 cancers in 185 countries. *CA: A Cancer Journal for Clinicians*. 2018; 68 (6) :394-424 . Available from: https://doi.org/10.3322/caac.21492
2. Cohen PA, Jhingran A, Oaknin A, Denny L. Cervical cancer. *The Lancet*. 2019; 393 (10167) :169-182 . Available from: https://doi.org/10.1016/s0140-6736(18)32470-x
3. Vodenkova S, Buchler T, Cervena K, Veskrnova V, Vodicka P, Vymetalkova V. 5-fluorouracil and other fluoropyrimidines in colorectal cancer: Past, present and future. *Pharmacology & Therapeutics*. 2020; 206 :107447 . Available from: https://doi.org/10.1016/j.pharmthera.2019.107447
4. Noordhuis P, Holwerda U, Van der Wilt CL, Van Groeningen CJ, Smid K, Meijer S, *et al*. 5-Fluorouracil incorporation into RNA and DNA in relation to thymidylate synthase inhibition of human colorectal cancers. *Annals of Oncology*. 2004; 15 (7) :1025-1032 . Available from: https://doi.org/10.1093/annonc/mdh264
5. Harutyunyan K, Nersesova L, Ayvazyan V, Avagyan E, Melkumyan M, Sargsyan M, *et al*. In silico and in vitro evaluation of drug-like properties and anticancer potential of novel 5-fluorouracil derivatives. *Scientific Reports*. 2025; 15 (1) . Available from: https://doi.org/10.1038/s41598-025-23237-y
6. Sethy C, Kundu CN. 5-Fluorouracil (5-FU) resistance and the new strategy to enhance the sensitivity against cancer: Implication of DNA repair inhibition. *Biomedicine & Pharmacotherapy*. 2021; 137 :111285 . Available from: https://doi.org/10.1016/j.biopha.2021.111285
7. Mitchell MJ, Billingsley MM, Haley RM, Wechsler ME, Peppas NA, Langer R. Engineering precision nanoparticles for drug delivery. *Nature Reviews Drug Discovery*. 2021; 20 (2) :101-124 . Available from: https://doi.org/10.1038/s41573-020-0090-8
8. Ulldemolins A, Seras-Franzoso J, Andrade F, Rafael D, Abasolo I, Gener P, *et al*. Perspectives of nano-carrier drug delivery systems to overcome cancer drug resistance in the clinics. *Cancer Drug Resistance*. 2021; 4 (1) :44 . Available from: https://doi.org/10.20517/cdr.2020.59
9. Saha S, Ali MR, Khaleque MA, Bacchu MS, Aly MA, Khan MZ. Metal oxide nanocarrier for targeted drug delivery towards the treatment of global infectious diseases: A review. *Journal of Drug Delivery Science and Technology*. 2023; 86 :104728 . Available from: https://doi.org/10.1016/j.jddst.2023.104728
10. Bonet-Aleta J, Calzada-Funes J, Hueso JL. Manganese oxide nano-platforms in cancer therapy: Recent advances on the development of synergistic strategies targeting the tumor microenvironment. *Applied Materials Today*. 2022; 29 :101628 . Available from: https://doi.org/10.1016/j.apmt.2022.101628
11. Ahmadi M, Ritter CA, von Woedtke T, Bekeschus S, Wende K. Package delivered: folate receptor-mediated transporters in cancer therapy and diagnosis. *Chemical Science*. 2024; 15 (6)

:1966-2006 . Available from: https://doi.org/10.1039/d3sc05539f

12. Ledermann JA, Canevari S, Thigpen T. Targeting the folate receptor: diagnostic and therapeutic approaches to personalize cancer treatments. *Annals of Oncology*. 2015; 26 (10) :2034-2043 . Available from: https://doi.org/10.1093/annonc/mdv250
13. Zhang J, Zhan B, Du Y, Liu N, Liu S, Li X. Targeted cancer treatment using folic acid-functionalized carbohydrate polymers: A new era in nanomedicine. *Industrial Crops and Products*. 2025; 235 :121704 . Available from: https://doi.org/10.1016/j.indcrop.2025.121704
14. Ibrahim MA, Othman R, Chessse CF, Ahmad Fisol F. Evaluation of Folate-Functionalized Nanoparticle Drug Delivery Systems—Effectiveness and Concerns. *Biomedicines*. 2023; 11 (7) :2080 . Available from: https://doi.org/10.3390/biomedicines11072080
15. Yallappa S, Manjanna J, Dhananjaya BL, Vishwanatha U, Ravishankar B, Gururaj H. Phytosynthesis of gold nanoparticles using *Mappia foetida* leaves extract and their conjugation with folic acid for delivery of doxorubicin to cancer cells. *Journal of Materials Science: Materials in Medicine*. 2015; 26 (9) :235 . Available from: https://doi.org/10.1007/s10856-015-5567-3
16. Liu W, Nie L, Li F, Aguilar ZP, Xu H, Xiong Y, *et al*. Folic acid conjugated magnetic iron oxide nanoparticles for nondestructive separation and detection of ovarian cancer cells from whole blood. *Biomaterials Science*. 2016; 4 (1) :159-166 . Available from: https://doi.org/10.1039/c5bm00207a
17. Mosmann T. Rapid colorimetric assay for cellular growth and survival: Application to proliferation and cytotoxicity assays. *Journal of Immunological Methods*. 1983; 65 (1-2) :55-63 . Available from: https://doi.org/10.1016/0022-1759(83)90303-4
18. Singh NP, McCoy MT, Tice RR, Schneider EL. A simple technique for quantitation of low levels of DNA damage in individual cells. *Experimental Cell Research*. 1988; 175 (1) :184-191 . Available from: https://doi.org/10.1016/0014-4827(88)90265-0
19. Patel S, Patel P, Bakshi SR. Titanium dioxide nanoparticles: an in vitro study of DNA binding, chromosome aberration assay, and comet assay. *Cytotechnology*. 2017; 69 (2) :245-263 . Available from: https://doi.org/10.1007/s10616-016-0054-3
20. Jonkman JE, Cathcart JA, Xu F, Bartolini ME, Amon JE, Stevens KM, *et al*. An introduction to the wound healing assay using live-cell microscopy. *Cell Adhesion & Migration*. 2014; 8 (5) :440-451 . Available from: https://doi.org/10.4161/cam.36224